Magnetic Moment Formation in Graphene Detected by Scattering of Pure Spin Currents

Kathleen M. McCreary,[1] Adrian G. Swartz,[1] Wei Han,[1] Jaroslav Fabian,[2] and Roland K. Kawakami[1,*]

[1]*Department of Physics and Astronomy, University of California, Riverside, California 92521, USA*

[2]*Institute for Theoretical Physics, University of Regensburg, D-93040 Regensburg, Germany*

(Received 20 July 2012; published 2 November 2012)

Hydrogen adatoms are shown to generate magnetic moments inside single layer graphene. Spin transport measurements on graphene spin valves exhibit a dip in the nonlocal spin signal as a function of the applied magnetic field, which is due to scattering (relaxation) of pure spin currents by exchange coupling to the magnetic moments. Furthermore, Hanle spin precession measurements indicate the presence of an exchange field generated by the magnetic moments. The entire experiment including spin transport is performed in an ultrahigh vacuum chamber, and the characteristic signatures of magnetic moment formation appear only after hydrogen adatoms are introduced. Lattice vacancies also demonstrate similar behavior indicating that the magnetic moment formation originates from p_z-orbital defects.

DOI: 10.1103/PhysRevLett.109.186604 PACS numbers: 72.80.Vp, 72.25.Rb, 75.30.Hx, 85.75.−d

Many fascinating predictions have been made regarding magnetism in graphene including the formation of magnetic moments from dopants, defects, and edges [1–8]. While several experimental techniques provide insight into this problem [9–21], lack of clear evidence for magnetic moment formation hinders development of this nascent field. Studies based on bulk magnetometry [9–16] directly measure magnetic properties, but because it measures the total magnetic moment (not just the signal from graphene) it is difficult to rule out artifacts from environmental magnetic impurities. Transport [17–19] and scanning tunneling microscopy [20,21] locally probe the graphene, but so far these measurements have been charge-based, so data are subject to various interpretations [22]. Thus, in order to convincingly demonstrate the formation of magnetic moments inside graphene due to dopants and defects, it is essential to employ techniques that directly probe the intrinsic spin degree of freedom of the magnetic moment while ensuring that the signal originates from the graphene sheet under investigation.

In this Letter, we utilize pure spin currents to demonstrate that hydrogen adatoms and lattice vacancies generate magnetic moments in single layer graphene. Pure spin currents are injected into graphene spin valve devices, and clear signatures of magnetic moment formation emerge in the nonlocal spin transport signal as hydrogen adatoms or lattice vacancies are systematically introduced in an ultrahigh vacuum environment. Specifically, introduction of these point defects generates a characteristic dip in the nonlocal signal as a function of the magnetic field. This feature is due to scattering (relaxation) of pure spin currents by localized magnetic moments in graphene and is explained quantitatively by a phenomenological theory based on spin-spin exchange coupling between conduction electrons and magnetic moments. Furthermore, we observe effective exchange fields due to this spin-spin coupling, which are of interest for novel phenomena and spintronic functionality [23–26] but have not been seen previously in graphene. Thus, these results provide the most clear and direct evidence for magnetic moment formation in graphene and demonstrate a method for utilizing localized magnetic moments to manipulate conduction electron spins.

For a systematic investigation, the spin transport measurement is first performed on a pristine single layer graphene (SLG) spin valve as a control measurement. Then, dopants or defects are controllably introduced to the SLG, and the measurement is repeated. The sample remains in ultrahigh vacuum during the entire process. Therefore, observed signatures of magnetic moment formation are caused by the adsorbed hydrogen or lattice vacancies.

Experiments are performed on nonlocal SLG spin valves [27–29] [Fig. 1(a)] consisting of two outer Au/Ti electrodes (a and d) and two ferromagnetic (FM) Co electrodes that make contact to SLG across MgO/TiO_2 tunnel barriers (b and c). The Co electrodes are capped with 5 nm Al_2O_3 to protect from hydrogen exposure. The tunnel barrier and capping layer are present only at the site of the FM electrodes, leaving the rest of the graphene uncovered. The device is fabricated on a SiO_2/Si substrate (300 nm thickness of SiO_2) where the Si is used as a back gate. Details of device fabrication are published elsewhere [29].

The charge and spin transport properties of pristine SLG spin valves are measured at 15 K by using lock-in techniques. The gate-dependent resistivity (ρ_G) of a representative sample A [black curve in Fig. 1(b)] exhibits a maximum at the gate voltage (V_G) of 0 V, which defines the Dirac point ($V_D = 0$ V). This sample exhibits a mobility (μ) of 6105 $cm^2/V\,s$. To investigate spin transport in the SLG device [Fig. 1(a)], a current (I) is applied between electrodes b and a, injecting spin-polarized carriers into graphene directly below the FM injector b. The spin population diffuses along the sample as a pure spin current (x axis), and the spin density is measured at the FM spin

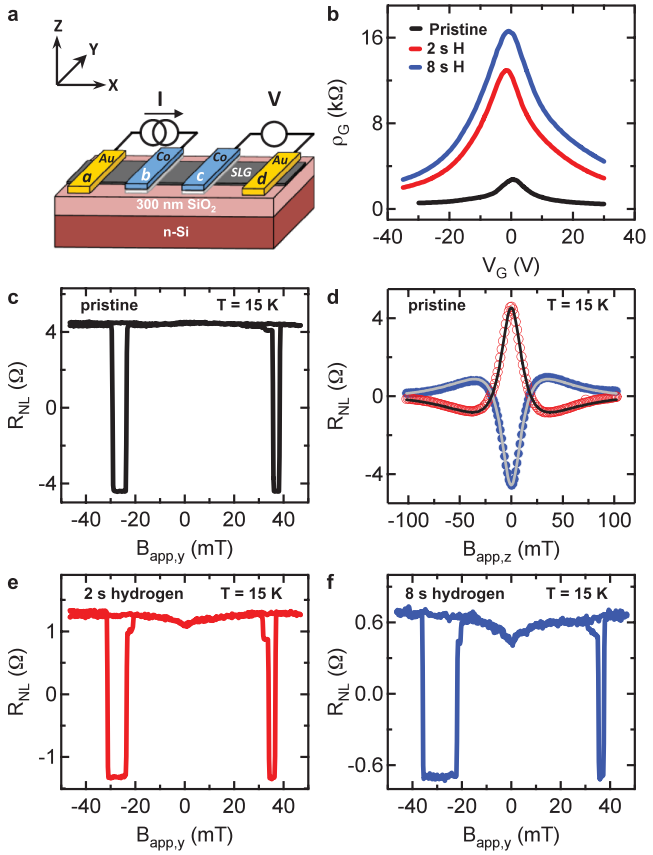

FIG. 1 (color). The effect of hydrogen exposure on charge and spin transport in SLG at 15 K. (a) Schematic illustration of the nonlocal spin valve device. (b) Gate-dependent resistivity for the pristine graphene (black curve) and following exposure to atomic hydrogen for 2 (red curve) and 8 s (blue curve). Upon hydrogen doping, the Dirac point shifts from 0 to -1 V. (c) Nonlocal spin transport measurement for pristine graphene. (d) Hanle spin precession measurement on pristine graphene. (e), (f) Nonlocal spin transport measurements after atomic hydrogen exposure for 2 and 8 s, respectively. Both curves exhibit a dip in R_{NL} at zero applied field, which is caused by spin relaxation induced by localized magnetic moments.

detector c as a voltage difference (V) between electrodes c and d. An applied magnetic field ($B_{\mathrm{app},y}$) along the electrode magnetization direction (y axis) is used to control the relative orientation of spin injector and detector magnetizations. For parallel alignment, the measured nonlocal resistance ($R_{\mathrm{NL}} = V/I$) is positive, whereas for antiparallel alignment R_{NL} is negative. The nonlocal spin signal is defined as the difference between parallel and antiparallel states ($\Delta R_{\mathrm{NL}} = R^{P}_{\mathrm{NL}} - R^{\mathrm{AP}}_{\mathrm{NL}}$). A typical scan of R_{NL} as a function of $B_{\mathrm{app},y}$ [Fig. 1(c)] displays discrete jumps as the electrode orientation changes between parallel and antiparallel. This sample exhibits a ΔR_{NL} of 8.8Ω (sample A with $V_G - V_D = -15$ V). A constant spin-independent background is subtracted from all R_{NL} data presented in this study. Out-of-plane magnetic fields are applied to generate spin precession, and the resulting data [Fig. 1(d); red for parallel, blue for antiparallel] are fit by the standard Hanle equation [28,29] (solid curves) to determine the spin lifetime ($\tau_{\mathrm{so}} = 479$ ps) and diffusion coefficient ($D = 0.023\ \mathrm{m}^2/\mathrm{s}$). The corresponding spin diffusion length is $\lambda = \sqrt{D\tau^{\mathrm{so}}} = 3.3\ \mu$m. Based on these values and a nonlocal spin signal of 8.8Ω, the spin polarization of the junction current (P_J) is calculated to be 20% [30,31].

Atomic hydrogen is introduced to spin valve devices at 15 K at a chamber pressure of 1×10^{-6} torr [31]. Following 2 s hydrogen exposure, the gate-dependent ρ_G [red curve in Fig. 1(b)] is dramatically increased. An additional 6 s of exposure (8 s total) further increases ρ_G [blue curve of Fig. 1(b)] and decreases the mobility to $495\ \mathrm{cm}^2/\mathrm{Vs}$. Based on the change in the resistivity, we make an order of magnitude estimate for the hydrogen coverage of 0.1% [31]. Accompanying the changes in charge transport are also changes in spin transport. Figures 1(e) and 1(f) display R_{NL} of sample A at $V_G - V_D = -15$ V as a function of $B_{\mathrm{app},y}$ following 2 and 8 s of exposure, respectively. The initial ΔR_{NL} of 8.8Ω is reduced to 2.6Ω after 2 s of hydrogen exposure and further reduced to 1.4Ω after 8 s. Interestingly, the R_{NL} scans exhibit a dip centered at zero applied field. The dip in R_{NL} is prevalent for both up and down sweeps of $B_{\mathrm{app},y}$ at all measured gate voltages and has been reproduced on multiple samples following hydrogen exposure. The ratio of the dip magnitude to ΔR_{NL} is found to increase with increasing hydrogen exposure [comparing Figs. 1(e) and 1(f)], indicating that the dip feature is dependent on the amount of adsorbed hydrogen.

To understand the origin of the dip in R_{NL}, we examine the expression for nonlocal resistance generated by spin transport [30]:

$$R_{\mathrm{NL}}^{(P/\mathrm{AP})} = \pm 2R_G e^{-L/\lambda} \prod_{i=1}^{2}\left(\frac{P_J \frac{R_i}{R_G}}{1-P_J^2} + \frac{P_F \frac{R_F}{R_G}}{1-P_F^2}\right) \times \left[\prod_{i=1}^{2}\left(1 + \frac{2\frac{R_i}{R_G}}{1-P_J^2} + \frac{2\frac{R_F}{R_G}}{1-P_F^2}\right) - e^{-2L/\lambda}\right]^{-1}, \quad (1)$$

where $R_G = \rho_G \lambda / w$ is the spin resistance of graphene, w is the graphene width, $R_F = \rho_F \lambda_F / A_J$ is the spin resistance of the cobalt, ρ_F is the cobalt resistivity, λ_F is the cobalt spin diffusion length, A_J is the junction area, P_F is the spin polarization of cobalt, R_1 and R_2 are the contact resistances of the spin injector and detector, respectively, and L is the distance from the injector to the detector. This equation shows that the spin density at the detector electrode depends on both charge and spin properties. First, we confirm that the SLG resistivity does not change with the magnetic field, so the dip is not related to changes in charge transport [31]. Second, we verify that the dip is not related to hydrogen-induced changes to the magnetic properties of the FM electrodes. Specifically, the effect of hydrogen

exposure is reversible upon thermal cycling to room temperature, and the anisotropic magnetoresistance of the Co electrodes is not affected by hydrogen exposure [31]. Next, we perform minor loop analysis on sample B [Fig. 2(a)] by reversing the magnetic field sweep immediately after the first magnetization reversal. The inversion of the dip in the antiparallel state (red curve) proves that the dip is due to increased spin relaxation at low fields. Furthermore, we rule out hyperfine coupling to nuclear spins as the origin of this increased spin relaxation [31].

As we discuss in the following, emergence of the dip following hydrogen adsorption identifies magnetic moment formation in graphene. The dip in R_{NL} is a characteristic feature of spin relaxation from exchange coupling with localized magnetic moments and can be illustrated from a simple textbook example of two coupled spins in a magnetic field. The Hamiltonian is given by $H = A_{\mathrm{ex}}\vec{S}_e \cdot \vec{S}_M + g_e\mu_B\vec{S}_e \cdot \vec{B}_{\mathrm{app}} + g_M\mu_B\vec{S}_M \cdot \vec{B}_{\mathrm{app}}$, where $\vec{S}_e$ is the conduction electron spin, $\vec{S}_M$ is the spin of the magnetic moment, g_e and g_M are the respective g factors, and A_{ex} is the exchange coupling strength [32,33]. Because of the presence of the exchange coupling, the individual spins are not conserved; only the total spin $\vec{S}_{\mathrm{tot}} = \vec{S}_e + \vec{S}_M$ is conserved. For the case where both $\vec{S}_e$ and $\vec{S}_M$ are spin-$\frac{1}{2}$, the quantum mechanical eigenstates in zero magnetic field are the well-known singlet ($S_{\mathrm{tot}} = 0$) and triplet ($S_{\mathrm{tot}} = 1$) spin states [34]. At higher magnetic fields the Zeeman terms dominate, and the two spins decouple so that the magnitudes and z components of $\vec{S}_e$ and $\vec{S}_M$ become good quantum numbers, similar to the Paschen-Back effect [34]. Thus, the dip in R_{NL} is qualitatively explained by the nonconservation of $\vec{S}_e$ at low fields due to the presence of exchange coupling with magnetic moments.

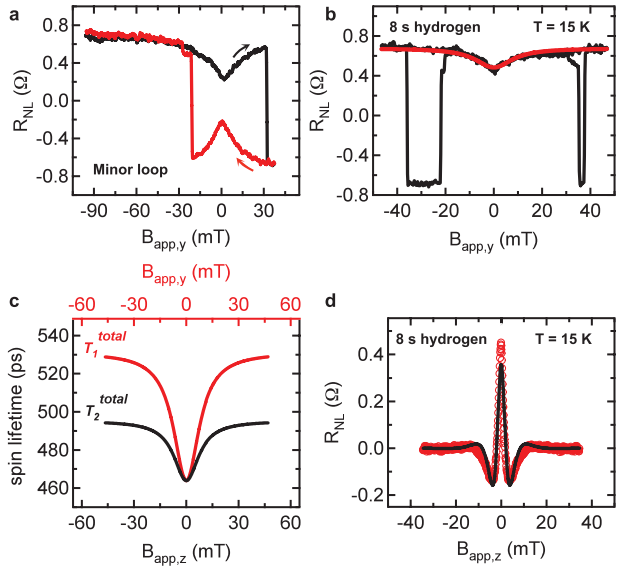

FIG. 2 (color). (a) A minor loop scan shows that the dip in R_{NL} for parallel alignment (black) becomes a peak for antiparallel alignment (red), indicating the feature is due to increased spin relaxation, as opposed to an artifact of the background level. (b) Fitting the dip in R_{NL} based on the model of spin relaxation by paramagnetic moments (data in black, fit in red). (c) Field dependence of longitudinal (red) and transverse (black) spin lifetimes. (d) Hanle precession data following 8 s hydrogen exposure (red) is fit using equation (3) (black curve).

To quantitatively analyze the experimental data, we must consider that a conduction electron will interact with many localized magnetic moments. Thus, the terms in the Hamiltonian involving the conduction electron are given by $H_e = \eta_M A_{\mathrm{ex}}\vec{S}_e \cdot \langle\vec{S}_M\rangle + g_e\mu_B\vec{S}_e \cdot \vec{B}_{\mathrm{app}} = g_e\mu_B\vec{S}_e \cdot (\bar{\vec{B}}_{\mathrm{ex}} + \vec{B}_{\mathrm{app}})$, where η_M is the filling density of magnetic moments. The averaging $\langle\ldots\rangle$ is over the ensemble of magnetic moments, and the effective field generated by the exchange interaction is $\bar{\vec{B}}_{\mathrm{ex}} = \frac{\eta_M A_{\mathrm{ex}}\langle\vec{S}_M\rangle}{g_e\mu_B}$. As the spins diffuse through the lattice, they experience varying magnetic moments which results in varying Larmor frequencies. In the local frame associated with the electrons, this can be described by a time-dependent, randomly fluctuating magnetic field $\vec{B}_{\mathrm{ex}}(t) = \bar{\vec{B}}_{\mathrm{ex}} + \Delta\vec{B}_{\mathrm{ex}}(t)$. For the R_{NL} measurements, the longitudinal spin relaxation due to a fluctuating field is given by [35]

$$\frac{1}{\tau_1^{\mathrm{ex}}} = \frac{(\Delta B)^2}{\tau_c}\frac{1}{(B_{\mathrm{app},y} + \bar{B}_{\mathrm{ex},y})^2 + (\frac{\hbar}{g_e\mu_B\tau_c})^2}, \qquad (2)$$

where ΔB is the rms fluctuation and τ_c is the correlation time [31]. The spin relaxation rate due to the exchange field is described by a Lorentzian curve which depends explicitly on the applied field $B_{\mathrm{app},y}$, resulting in strong spin relaxation at low fields and suppressed spin relaxation at high fields. Because of the presence of $\bar{B}_{\mathrm{ex},y}$ in Eq. (2), ferromagnetic ordering will produce a dip in R_{NL} that is centered away from zero and is hysteretic, while paramagnetic ordering will produce a nonhysteretic dip centered at zero field. Thus, the magnetic moments measured in these experiments are paramagnetic. The total longitudinal spin lifetime T_1^{total} of conduction electrons is dependent on both the usual spin relaxation due to spin orbit coupling (τ_{so}) and longitudinal spin relaxation from the exchange field (τ_1^{ex}), such that $(T_1^{\mathrm{total}})^{-1} = (\tau_1^{\mathrm{ex}})^{-1} + (\tau^{\mathrm{so}})^{-1}$. We apply the above model to the nonlocal spin transport data presented in Fig. 1(f) (sample A) and fit by using Eq. (1), $\lambda = \sqrt{DT_1^{\mathrm{total}}}$, and Eq. (2) [31]. The resulting fit [red line in Fig. 2(b)] replicates the shape and magnitude of the dip measured in R_{NL} [black line in Fig. 2(b)]. The field-dependent T_1^{total} [Fig. 2(c)] exhibits a minimum of 464 ps at zero field and increases asymptotically towards $\tau_{\mathrm{so}} =$ 531 ps for large $B_{\mathrm{app},y}$. The values obtained for ΔB and τ_c are 6.78 mT and 192 ps, respectively. The field-dependent spin relaxation following atomic hydrogen exposure,

which emerges as a dip in R_{NL}, is a clear signature of paramagnetic moment formation.

Spin precession measurements provide further evidence for the presence of magnetic moments. Figure 2(d) shows spin precession data for sample A (8 s exposure, $V_G - V_D = -15$ V) with FM electrodes in the parallel alignment state. The Hanle curve has considerably narrowed compared to the precession measurements obtained prior to hydrogen adsorption [Fig. 1(d)]. The sharpening of the Hanle curve results from the presence of an exchange field. The injected spins precess around a total field $B_{\mathrm{tot}} = B_{\mathrm{app},z} + \bar{B}_{\mathrm{ex},z}$ (along the z axis) that includes not only the applied field but also the exchange field from the paramagnetic moments. At 15 K and $B_{\mathrm{app},z} < 100$ mT, the magnetization is proportional to the applied field so that $\bar{B}_{\mathrm{ex},z} = kB_{\mathrm{app},z}$, where k is a proportionality constant. Thus, the spins precess about B_{tot} with frequency $\omega = g_e\mu_B B_{\mathrm{tot}}/\hbar = g_e(1+k)\mu_B B_{\mathrm{app},z}/\hbar = g_e^*\mu_B B_{\mathrm{app},z}/\hbar$. To properly account for the enhanced g factor induced by the magnetic moments, the Hanle equation must be modified to

$$R_{\mathrm{NL}} = S\int_0^\infty \frac{e^{-L^2/4Dt}}{\sqrt{4\pi Dt}}\cos\left(\frac{g_e^*\mu_B B_{\mathrm{app},z}t}{\hbar}\right)e^{-t/T_2^{\mathrm{total}}}dt, \quad (3)$$

where T_2^{total} is the transverse spin lifetime. As shown in Fig. 2(c), the T_2^{total} is related to, but different from, T_1^{total} [31]. Using the field-dependent T_2^{total}, the precession data [red circles in Fig. 2(d)] is fit to Eq. (3) (black line) to yield a value of $g_e^* = 7.13$. Physically, $g_e^* > 2$ corresponds to an enhanced spin precession frequency resulting from the exchange field. A detailed discussion of the Hanle fitting and the gate-dependent properties of the exchange field are provided in the Supplemental Material [31]. The dramatic narrowing of the Hanle peak combined with the emergence of a dip in R_{NL} provides the most direct evidence to date for the formation of magnetic moments in graphene due to the adsorption of atomic hydrogen.

We now turn our attention to lattice vacancy defects in graphene. Several theoretical works suggest the similarity of magnetism due to vacancies and hydrogen doping [1,4], as both should create magnetic moments inside graphene due to the removal or hybridization of p_z orbitals. To produce lattice vacancies in pristine SLG spin valves, we perform Ar sputtering at low energies and examine the subsequent nonlocal spin transport. We again observe the emergence of a dip in R_{NL} and narrowed Hanle curve, indicating the formation of paramagnetic moments in graphene [31]. Given the very different chemical and structural properties of lattice vacancies compared to adsorbed hydrogen, the observation of similar features in the spin transport data provides strong evidence that the magnetic moments are created by the removal of p_z orbitals from the π band, as predicted theoretically.

In conclusion, clear signatures of magnetic moment formation are observed in both the nonlocal spin transport and Hanle precession data, which emerge only after exposure to atomic hydrogen or lattice vacancies. The results and techniques presented here are important for future developments in magnetism and spintronics.

We acknowledge Z. Zhao and C. N. Lau for their technical assistance and support from NSF (DMR-1007057, MRSEC DMR-0820414), ONR (N00014-12-1-0469), NRI-NSF (NEB-1124601), and DFG (SFB 689). K. M. M. and A. G. S. contributed equally to this work.

*roland.kawakami@ucr.edu

[1] O. V. Yazyev and L. Helm, Phys. Rev. B **75**, 125408 (2007).
[2] D. W. Boukhvalov, M. I. Katsnelson, and A. I. Lichtenstein, Phys. Rev. B **77**, 035427 (2008).
[3] J. Zhou, Q. Wang, Q. Sun, X. S. Chen, Y. Kawazoe, and P. Jena, Nano Lett. **9**, 3867 (2009).
[4] D. Soriano, N. Leconte, P. Ordejon, J.-C. Charlier, J.-J. Palacios, and S. Roche, Phys. Rev. Lett. **107**, 016602 (2011).
[5] B. Uchoa, V. N. Kotov, N. M. R. Peres, and A. H. Castro Neto, Phys. Rev. Lett. **101**, 026805 (2008).
[6] M. A. H. Vozmediano, M. P. López-Sancho, T. Stauber, and F. Guinea, Phys. Rev. B **72**, 155121 (2005).
[7] L. Pisani, J. A. Chan, B. Montanari, and N. M. Harrison, Phys. Rev. B **75**, 064418 (2007).
[8] H. Lee, Y.-W. Son, N. Park, S. Han, and J. Yu, Phys. Rev. B **72**, 174431 (2005).
[9] R. R. Nair, M. Sepioni, I.-L. Tsai, O. Lehtinen, J. Keinonen, A. V. Krasheninnikov, T. Thomson, A. K. Geim, and I. V. Grigorieva, Nat. Phys. **8**, 199 (2012).
[10] O. Yazyev, Rep. Prog. Phys. **73**, 056501 (2010).
[11] M. Sepioni, R. R. Nair, S. Rablen, J. Narayanan, F. Tuna, R. Winpenny, A. K. Geim, and I. V. Grigorieva, Phys. Rev. Lett. **105**, 207205 (2010).
[12] Y. Wang, Y. Huang, Y. Song, X. Zhang, Y. Ma, J. Liang, and Y. Chen, Nano Lett. **9**, 220 (2009).
[13] H. S. S. Ramakrishna Matte, K. S. Subrahmanyam, and C. N. R. Rao, J. Phys. Chem. C **113**, 9982 (2009).
[14] L. Xie, *et al.*, Appl. Phys. Lett. **98**, 193113 (2011).
[15] P. Esquinazi, D. Spemann, R. Hohne, A. Setzer, K.-H. Han, and T. Butz, Phys. Rev. Lett. **91**, 227201 (2003).
[16] J. Cervenka, M. I. Katsnelson, and C. F. J. Flipse, Nat. Phys. **5**, 840 (2009).
[17] A. Candini, C. Alvino, W. Wernsdorfer, and M. Affronte, Phys. Rev. B **83**, 121401 (2011).
[18] J.-H. Chen, L. Li, W. G. Cullen, E. D. Williams, and M. S. Fuhrer, Nat. Phys. **7**, 535 (2011).
[19] X. Hong, S.-H. Cheng, C. Herding, and J. Zhu, Phys. Rev. B **83**, 085410 (2011).
[20] M. M. Ugeda, I. Brihuega, F. Guinea, and J. M. Gomez-Rodriguez, Phys. Rev. Lett. **104**, 096804 (2010).
[21] C. Tao, L. Jiao, O. V. Yazyev, Y.-C. Chen, J. Feng, X. Zhang, R. B. Capaz, J. M. Tour, A. Zettl, S. G. Louie, H. Dai, and M. F. Crommie, Nat. Phys. **7**, 616 (2011).
[22] J. Jobst and H. B. Weber, Nat. Phys. **8**, 352 (2012).
[23] H. Haugen, D. Huertas-Hernando, and A. Brataas, Phys. Rev. B **77**, 115406 (2008).

[24] Y. G. Semenov, K. W. Kim, and J. M. Zavada, Appl. Phys. Lett. **91**, 153105 (2007).
[25] P. Michetti, P. Recher, and G. Iannaccone, Nano Lett. **10**, 4463 (2010).
[26] Z. Qiao, S. A. Yang, W. Feng, W.-K. Tse, J. Ding, Y. Yao, J. Wang, and Q. Niu, Phys. Rev. B **82**, 161414 (2010).
[27] M. Johnson and R. H. Silsbee, Phys. Rev. Lett. **55**, 1790 (1985).
[28] N. Tombros, C. Jozsa, M. Popinciuc, H. T. Jonkman, and B. J. van Wees, Nature (London) **448**, 571 (2007).
[29] W. Han, K. M. McCreary, K. Pi, W. H. Wang, Y. Li, H. Wen, J. R. Chen, and R. K. Kawakami, J. Magn. Magn. Mater. **324**, 369 (2012).
[30] S. Takahashi and S. Maekawa, Phys. Rev. B **67**, 052409 (2003).
[31] See Supplemental Material at http://link.aps.org/supplemental/10.1103/PhysRevLett.109.186604 for control measurements, details of analysis, and results for lattice vacancies.
[32] J. K. Furdyna, J. Appl. Phys. **64**, R29 (1988).
[33] G. Bastard and R. Ferreira, Surf. Sci. **267**, 335 (1992).
[34] D. Griffiths, *Introduction to Quantum Mechanics* (Pearson Prentice Hall, Upper Saddle River, NJ, 2005), 2nd ed.
[35] J. Fabian, A. Matos-Abiague, C. Ertler, P. Stano, and I. Zutic, Acta Phys. Slovaca **57**, 565 (2007).